ADVANCED ENERGY MATERIALS
www.advenergymat.de

Highly Efficient Perovskite Solar Cells Enabled by Multiple Ligand Passivation

*Zhifang Wu, Maowei Jiang, Zonghao Liu, Afshan Jamshaid, Luis K. Ono, and Yabing Qi**

In the past decade, the efficiency of perovskite solar cells quickly increased from 3.8% to 25.2%. The quality of perovskite films plays vital role in device performance. The films fabricated by solution-process are usually polycrystalline, with significantly higher defect density than that of single crystal. One kind of defect in the films is uncoordinated Pb^{2+}, which is usually generated during thermal annealing process due to the volatile organic component. Another detrimental kind of defect is Pb^0, which is often observed during the film fabrication process or solar cell operation. Because the open circuit voltage has a close relation with the defect density, it is thus desirable to passivate these two kinds of defects. Here, a molecule with multiple ligands is introduced, which not only passivates the uncoordinated Pb^{2+} defects, but also suppresses the formation of Pb^0 defects. Meanwhile, such a treatment improves the energy level alignment between the valence band of perovskite and the highest occupied molecular orbital of spiro-OMeTAD. As a result, the performance of perovskite solar cells significantly increases from 19.0% to 21.4%.

1. Introduction

In the past decade, the power conversion efficiency (PCE) of perovskite based solar cells increased quickly from 3.8%[1] to the current record of 25.2%.[2] Several factors affect the performance of perovskite solar cells, such as the perovskite film quality and interfacial charge transport.[3] It is reported that the defect density of poly-crystalline perovskite is significantly higher than that of single crystal perovskite.[4] During the thermal annealing process, the organic volatile component tends to escape from perovskite leaving behind the uncoordinated Pb^{2+} defect, which serves as recombination sites.[5] It is also reported that Pb^0 species is another detrimental kind of defect, which is usually generated during perovskite solar cell fabrication and operation. Therefore, Pb-related defects in perovskite deteriorate not only the device stability, but also PCE.[6] Defect passivation (or defect engineering) has been widely investigated as an effective way to heal defects in perovskite and suppress the nonradiative recombination dynamics. In terms of the interface charge transport, mismatched interface energy level alignment may be detrimental to the device performance.[7] 2,2′,7,7′-Tetrakis[*N*,*N*-di(4-methoxyphenyl)amino]-9,9′-spirobifluorene (spiro-OMeTAD) is a widely employed hole transport material (HTM), which is able to deliver a high PCE.[8] However, it is found that there is a large energy level mismatch between the highest occupied molecular orbital (HOMO) of spiro-OMeTAD and valence band maximum (VBM) of perovskite.[9] To maximize the hole extraction efficiency, interface energy level alignment should be optimized. Due to the mature recipe of spiro-OMeTAD doped with bis(trifluoromethane)sulfonimide lithium (Li-TFSI) and 4-*tert*-butylpyridine (TBP), we focus on fine tuning of electronic properties of the perovskite side of the perovskite/spiro-OMeTAD interface. Here a molecule with multiple ligands called pentaerythritol tetrakis(3-mercaptopropionate) (denoted as ML) is used to modify the perovskite surface because of the following advantages: 1) ML effectively passivates the uncoordinated Pb^{2+} defects via Lewis acid–base interaction; 2) this material is found to be able to suppress the formation of Pb^0 defects; 3) ML simultaneously modulates the interfacial electronic property of perovskite, leading to a better match of interfacial energy level alignment at the interface between the perovskite and spiro-OMeTAD HTM. Previously, most attention was paid to passivation of single halide vacancies instead of double or triple halide vacancies. In a recent study,[10] our group confirmed experimentally the presence of double and triple halide vacancies at the surface of perovskite. Due to the steric effect, it will be more efficient to use the multiple-ligand (pentaerythritol tetrakis (3-mercaptopropionate)) to passivate the double or triple ligand, instead of using the mono-ligand (mercaptoacetate). Also, the stability of the metal–ligand complex increases when the mono-ligand is replaced by the multiligand due to the chelate effect.

2. Results and Discussion

$FA_{0.82}MA_{0.13}Cs_{0.05}PbI_{2.87}Br_{0.13}$ perovskite films are fabricated by the two-step inter-diffusion method using the reported

Dr. Z. Wu, Dr. M. Jiang, Dr. Z. Liu, A. Jamshaid, Dr. L. K. Ono, Prof. Y. B. Qi
Energy Materials and Surface Sciences Unit (EMSSU)
Okinawa Institute of Science and Technology Graduate University (OIST)
1919-1 Tancha, Onna-son, Kunigami-gun, Okinawa 904-0495, Japan
E-mail: Yabing.Qi@OIST.jp

The ORCID identification number(s) for the author(s) of this article can be found under https://doi.org/10.1002/aenm.201903696.

DOI: 10.1002/aenm.201903696

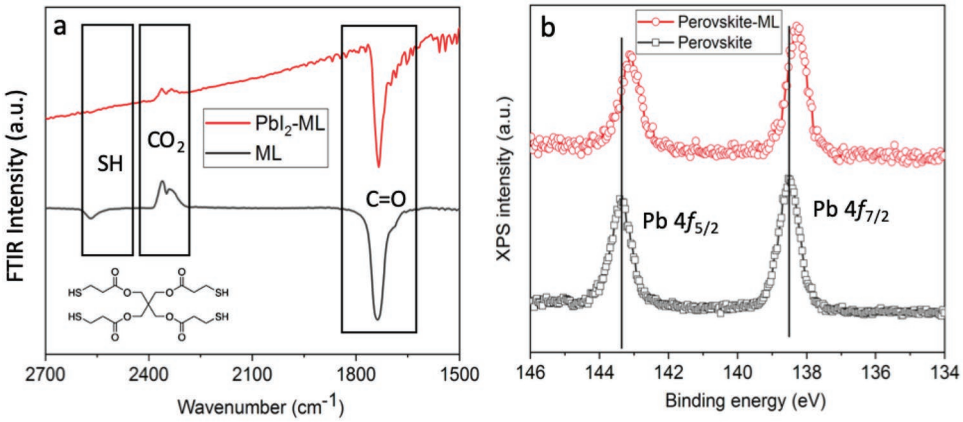

Figure 1. a) Normalized FTIR spectra of ML and PbI_2-ML ligand complex. b) XPS spectra and comparison of binding energies corresponding to the Pb-4f core level of perovskite and perovskite-ML complex. Inset in (a) shows the molecular structure of ML ligand.

procedure.[8] ML modified perovskite films (perovskite/ML) are prepared by spin-coating the ML solution on substrates followed by thermal annealing and a washing process. There is no obvious change in XRD peaks after ML modification (Figure S1, Supporting Information). Also, there is no obvious difference in surface morphology (Figure S2, Supporting Information). The excessive PbI_2 evidenced by SEM and XRD is proposed by several studies to be beneficial for device performance.[11]

We investigated the interaction between Pb^{2+} and ML ligand by Fourier-transform infrared spectroscopy (FTIR). As shown in the **Figure 1**a and Figure S3 (Supporting Information), the CO_2 related peaks with wavenumbers at 2361 and 2333 cm^{-1} are observed due to the unavoidable exposure to air. The peak corresponding to the C=O stretching vibrational mode is determined to be at 1734 cm^{-1}. The disappearance of the characteristic peak of thiol group (SH) at around 2568 cm^{-1} indicates the strong interaction of the SH ligand with PbI_2 via the Lewis acid–base interaction. X-ray photoelectron spectroscopy (XPS) is further used to investigate the binding energy changes of uncoordinated Pb^{2+}. Due to the electron-donating nature of the Lewis base, the $Pb^{\delta+}$ peak of the perovskite-ML complex is observed to shift toward a lower binding energy (Figure 1b), corroborating the interaction between uncoordinated Pb^{2+} and the SH ligand.

Time-resolved photoluminescence (TRPL) is used to investigate the charge recombination of perovskite (**Figure 2**a). We chose a bi-exponential function to fit the curves, where τ_i represents time constant of exponential component, A_i refers to the fractional amplitude for each exponential[12]

$$I_{PL} = A_1 \exp(-t/\tau_1) + A_2 \exp(-t/\tau_2) \quad (1)$$

τ_{av} refers to the amplitude-weighted average lifetimes, which can be given by the equation below[12]

$$\tau_{av} = A_1 * \tau_1 + A_2 * \tau_2 \quad (2)$$

Fractional contribution (f_i) of each decay time to the whole time can be calculated by the following equation[12]

$$f_i = \frac{A_i * \tau_i}{\sum_j A_j * \tau_j} \quad (3)$$

The TRPL spectrum indicates a fast- (τ_1) and a slow-decay (τ_2) component.[11] The slow decay component τ_2 is attributed to radiative recombination of free carriers, which is mainly associated with charge transfer across the interface.[13] The fast-decay component is assigned to trap-assisted nonradiative recombination at the interface.[13] Figure 2a and Table S1 (Supporting Information) show that τ_{av} of TRPL for the perovskite/ML and the control is 184.84 and 143.28 ns, respectively. Table S1 (Supporting Information) shows that τ_1 of the perovskite-ML is determined to be 20.14 ns, similar to that of the control sample (i.e., without the ML ligand) (21.71 ns). However, A_1 of perovskite/ML is estimated to be 0.045, which is significantly lower than that of control film

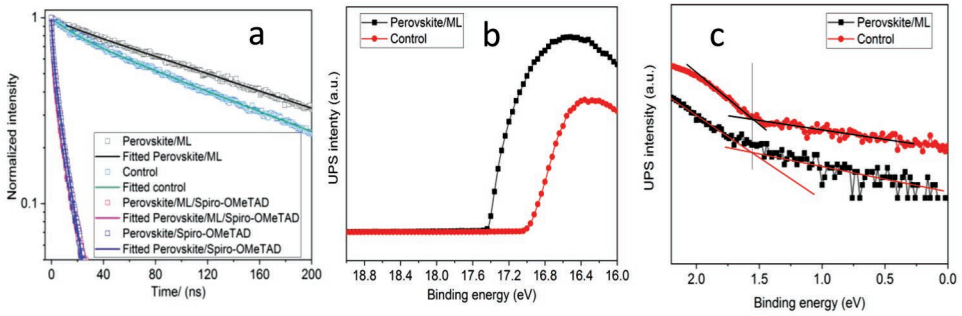

Figure 2. a) TRPL spectra of perovskite samples with the ML ligand passivation (Perovskite/ML) and without (Control) and with/without spiro-OMeTAD, b) UPS spectra (He–Iα = 21.22 eV) of the secondary electron cutoff onset region of control perovskite and perovskite-ML complex and c) the valence band maximum region with respect to the Femi level of perovskite with and without the ML ligand modification.

(0.148), indicating that the surface recombination is effectively suppressed in the case of the ligand modified perovskite.

Ultraviolet photoemission spectroscopy (UPS) is used to investigate the electronic property of perovskite. Figure 2b shows that the work function (WF) of perovskite/ML is 3.79 eV and the valence band maximum is 1.58 eV, yielding an ionization energy (IE) of 5.37 eV. The corresponding WF and VBM of control perovskite is 4.22 and 1.55 eV, leading to an IE of 5.77 eV. The HOMO of spiro-OMeTAD is around 5.2 eV.[14] Thus, the energy barrier between the perovskite and spiro-OMeTAD is reduced from 0.57 to 0.17 eV after multiple ligand passivation. To check whether the reduced energy barrier between IE of perovskite and HOMO of spiro-OMeTAD helps improve the hole extraction efficiency, the lifetime of perovskite coated with spiro-OMeTAD in the presence/absence of ligand is measured. Figure 2a and Table S2 (Supporting Information) show that the lifetime of perovskite/ML/spiro-OMeTAD is evaluated to be 4.28 ns, which is slightly lower than that of perovskite/spiro-OMeTAD (5.07 ns). The third τ value denoted as $\tau_{1/e}$ corresponds to the lifetime determined using the definition of PL lifetime (i.e., the time when the PL intensity decrease to 1/e of the initial intensity). The $\tau_{1/e}$ of perovskite/ML and the control is determined to be 178.56 and 134.19 ns, respectively, which is consistent with the extracted lifetime using bi-exponential function. The $\tau_{1/e}$ value derived from perovskite/spiro-OMeTAD samples is used to compare with the lifetime of bare perovskite so that we can determine the efficiency of interface hole extraction. For example, we normalize the initial PL lifetime of the bare perovskite film to 1 (Table S2, Supporting Information). The relative PL lifetime of perovskite/spiro-OMeTAD is determined to be 3.78% with respect to the bare perovskite film (Table S2, Supporting Information). The corresponding relative PL lifetime of perovskite/ML/spiro-OMeTAD is determined to be 2.4% with respect to the perovskite/ML film. The reduction of relative PL lifetime from 3.78% to 2.4% after ML ligand passivation, indicates that the ML ligand modification facilitates interface hole extraction, which is ascribed to the better matching of interfacial energy level alignment. Compared with perovskite/spiro-OMeTAD, the lifetime of perovskite/ML/spiro-OMeTAD quenches 1.58 times faster (Table S2, Supporting Information), indicating the enhancement of hole extraction, which is ascribed to the better match of energy alignment between the perovskite and spiro-OMeTAD.[15]

XPS is used to investigate the surface composition of perovskite/ML (**Figure 3**a and Figure S4, Supporting Information). The XPS peaks with binding energies at 532.64

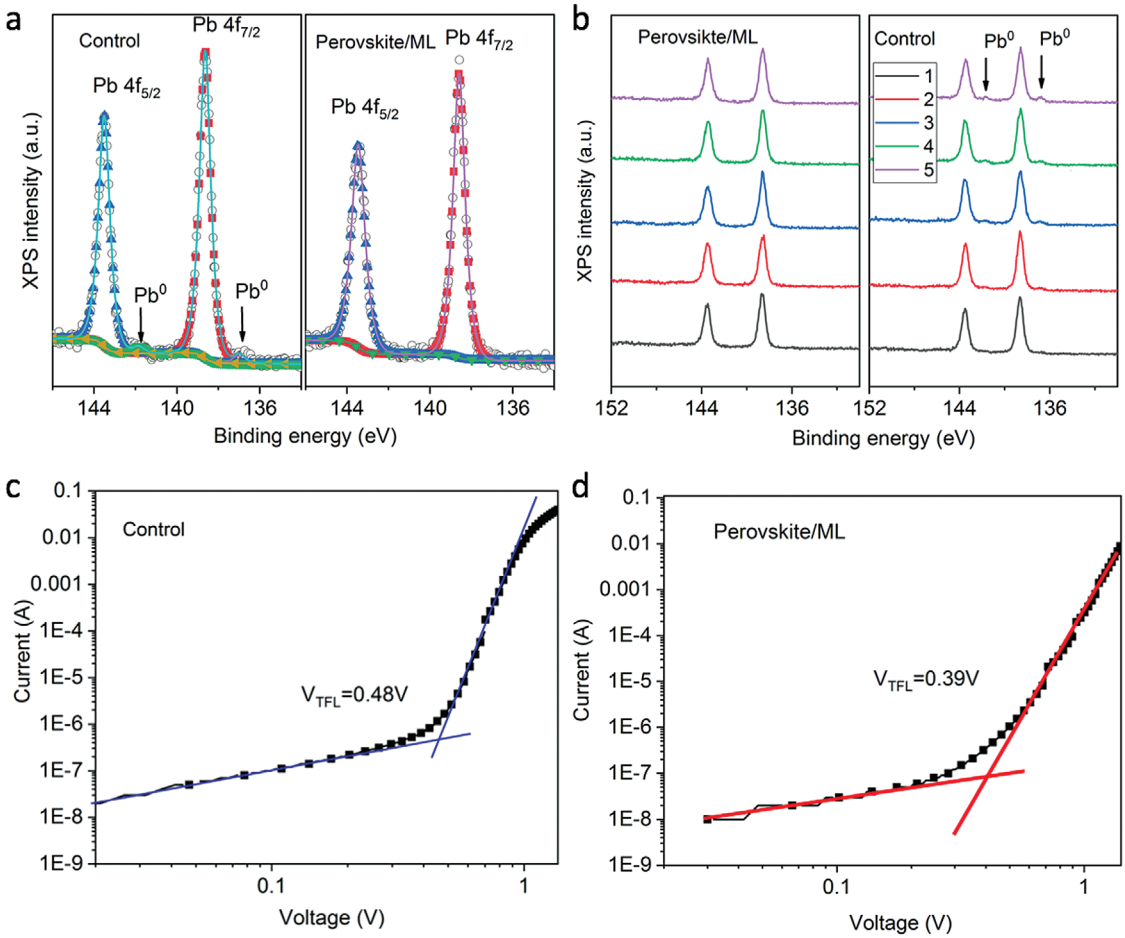

Figure 3. a) XPS spectra (Al–Kα = 1486.6 eV) of the Pb-4f core levels of perovskite derived from the first scan. b) Evolution of Pb^0 monitored by XPS during 5 consecutive scans. c,d) SCLC spectra for the two kinds of devices: c) perovskite without ML ligands (Control) and d) perovskite with ML ligands (Perovskite/ML).

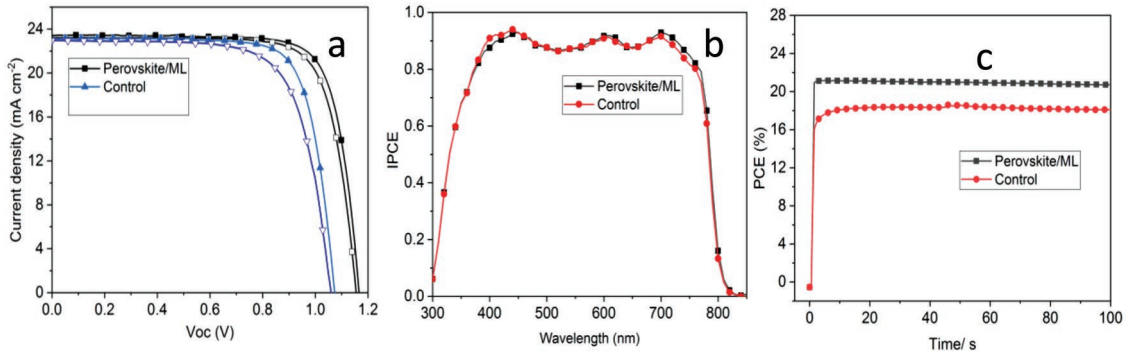

Figure 4. a) Current density–voltage (*J*–*V*) curves, b) IPCE, and c) steady-state PCE output of perovskite solar cells corresponding to perovskites with the ML passivation (perovskite/ML) and without the ML passivation (Control).

and 534.09 eV are assigned to O-1s in the C=O group and O atom adjacent to C=O in the ML molecule (Figure S4b, Supporting Information).[16] Figure S4a (Supporting Information) shows the peaks corresponding to S-2$p_{3/2}$ and S-2$p_{1/2}$ with binding energies at 165.29 and 164.13 eV, respectively.[17] The Pb^{2+}-4$f_{7/2}$ and Pb^{2+}-4$f_{5/2}$ peaks derived from the first scan is determined to be 143.51 and 138.63 eV, respectively (Figure 3a). Interestingly, the Pb^0 species, which is found in the control sample disappears after ligand passivation. More importantly, Figure 3b shows that the amount of Pb^0 species in the control sample continues to increase upon the consecutive five XPS scans. However, Pb^0 is not observed in perovskite/ML even after five scans, confirming again that the ligand is able to suppress the formation of Pb^0. The mechanism how the ligand passivation is able to suppress the formation of Pb^0 species, is important to further explore the appropriate passivation material. The suppressed formation of Pb^0 is correlated with back-oxidation of Pb^0 to Pb^{2+} species in the presence of passivating molecules. Although the thiol group (SH) of the ML ligand shows the reduction properties, in the presence of O_2, two thiol groups are able to connect to each other to form a disulfide[18] intermediate compound (R-S-S-R, R represents alkyl group), which shows oxidation properties. Thus, we hypothesize that this disulfide intermediate compound is the cause for oxidation of Pb^0 to Pb^{2+}. To verity this hypothesis, we measured the binding energy of S by XPS. The binding energy of S in the thiol group SH is expected to be around 163.8 ± 0.4[19] and the binding energy of R-S-S-R is expected to be around 164.0 ± 0.5.[19] On the basis of the careful analysis of the XPS results (Figure S4, Supporting Information) by taking into account: 1) binding energy shifts when the SH and R-S-S-R coordinate with Pb^{2+} and 2) the proximity of the peak positions, our S-2p XPS spectra suggest the formation of R-S-S-R intermediate. Furthermore, the comparison of our Pb-4f XPS spectra for bare perovskite and perovskite/ML systems (**Figure 4**a,b) shows that the Pb^0 species is significantly suppressed in the case of the perovskite/ML films, while Pb^0 is present in the case of the bare perovskite films. Suppression of the formation of Pb^0 helps reduce nonradiative recombination, which is consistent with the observed longer lifetime of perovskite/ML. We further evaluate the defect density of the film using the space-charge limited current (SCLC) method (Figure 3c,d) with the device configuration of ITO/perovskite/Au according to the following equation[20]

$$N_t = \frac{2\varepsilon\,\varepsilon_0 V_{TFL}}{eL^2} \tag{4}$$

where ε and ε_0 are the dielectric constants of perovskite and the vacuum permittivity, respectively, V_{TFL} is trap-filled limit voltage, L is the thickness of the perovskite films, and e is the elementary charge. The defect density of Perovskite/ML is evaluated to be 2.57×10^{15} cm^{-3}, which is 18.7% lower than that of the control sample (3.17×10^{15} cm^{-3}), indicating the improved perovskite film quality after ligand passivation.

Figure 4 and **Table 1** show that PCE of the best performing perovskite/ML increases from 19.0% to 21.4% with an open circuit voltage (V_{oc}) of 1.16 V, current density (J_{sc}) of 23.5 mA cm^{-2} and fill factor (FF) of 78.6%. The corresponding steady-state output is 20.9%. In addition, the steady state output of the ligand modified device rises more swiftly than that of control device, indicating the much faster charge collection in this device.[9,21] This observation is in good agreement with better matched energy level alignments. Furthermore, the higher incident photon-to-electron conversion efficiency (IPCE) of perovskite/ML also corroborates the better energy level alignment between VBM of perovskite and HOMO of spiro-OMeTAD. The deviation of the slope from k_BT/q is reported to reflect defect-assisted recombination in the devices.[8,21] As shown in Figure S5 (Supporting Information), light intensity-dependent V_{oc} measurement respectively reveals a slope of 1.44 and 1.76 for the perovskite/ML and Control samples, implying the defect-assisted

Table 1. Photovoltaic parameter of cells based on two kinds: perovskites with the ML passivation (perovskite/ML) and without the ML passivation (Control).

PSCs	Scan direction	V_{oc} [V]	J_{sc} [mA cm^{-2}]	FF [%]	Efficiency [%]	Steady-state output
Perovskite/ML	Reverse	1.16	23.5	78.6	21.4%	20.9%
	Forward	1.15	23.2	76.7	20.6%	
Control	Reverse	1.07	23.1	76.5	19.0%	18.4%
	Forward	1.06	23.0	71.3	17.3%	

recombination is suppressed after introduction of multiple ligand. Figure S6 (Supporting Information) and Table S3 (Supporting Information) show the average V_{oc} of perovskite/ML from 30 devices is 1.13 V, which is 80 mV higher than that of perovskite/control. Figure S7 (Supporting Information) shows the statistical analysis of PCE for the ligand-modified and control devices. These results confirm again that the above-mentioned nonradiative recombination in perovskite/ML is suppressed.

The stability of perovskite solar cell is important for commercialization. We track the humidity stability of perovskite under high humidity (around 70%). After being aged for 96 h, the statistical analyses of the device data show that the perovskite/ML and the control device retains 70.6% and 58.7% of starting PCE, respectively (Figure S8, Supporting Information). This result suggests that the insertion of thin passivation layer also mildly helps improve the humidity stability.

3. Conclusion

In conclusion, we introduced a molecule with multiple ligands to modify the perovskite film of perovskite/spiro-OMeTAD interface, and successfully modulated the interface energy level alignment between perovskite and HTM to achieve efficient charge transfer. At the same time, two kinds of defects (uncoordinated Pb^{2+} and Pb^0) are effectively suppressed. As a result, the PCE of ligand passivated device increases from 19.0% to 21.4%. Our work provides a comprehensive approach to further improve the efficiency of perovskite solar cells.

Supporting Information

Supporting Information is available from the Wiley Online Library or from the author.

Acknowledgements

This work was supported by funding from the Energy Materials and Surface Sciences Unit of the Okinawa Institute of Science and Technology Graduate University, the OIST R&D Cluster Research Program, the OIST Proof of Concept (POC) Program, and JSPS KAKENHI Grant Number JP18K05266.

Conflict of Interest

The authors declare no conflict of interest.

Keywords

defects, efficiency, energy level alignment, passivation, perovskite solar cells

Received: November 10, 2019
Revised: December 29, 2019
Published online: February 3, 2020

[1] A. Kojima, K. Teshima, Y. Shirai, T. Miyasaka, *J. Am. Chem. Soc.* **2009**, *131*, 6050.
[2] https://www.nrel.gov/pv/cell-efficiency.html, (accessed: August 2019).
[3] a) S. G. Motti, D. Meggiolaro, A. J. Barker, E. Mosconi, C. A. R. Perini, J. M. Ball, M. Gandini, M. Kim, F. De Angelis, A. Petrozza, *Nat. Photonics* **2019**, *13*, 532; b) D. Luo, W. Yang, Z. Wang, A. Sadhanala, Q. Hu, R. Su, R. Shivanna, G. F. Trindade, J. F. Watts, Z. Xu, T. Liu, K. Chen, F. Ye, P. Wu, L. Zhao, J. Wu, Y. Tu, Y. Zhang, X. Yang, W. Zhang, R. H. Friend, Q. Gong, H. J. Snaith, R. Zhu, *Science* **2018**, *360*, 1442; c) Y. Shao, Z. Xiao, C. Bi, Y. Yuan, J. Huang, *Nat. Commun.* **2014**, *5*, 5784; d) W. S. Yang, B.-W. Park, E. H. Jung, N. J. Jeon, Y. C. Kim, D. U. Lee, S. S. Shin, J. Seo, E. K. Kim, J. H. Noh, S. I. Seok, *Science* **2017**, *356*, 1376.
[4] W. Peng, X. Miao, V. Adinolfi, E. Alarousu, O. El Tall, A. H. Emwas, C. Zhao, G. Walters, J. Liu, O. Ouellette, *Angew. Chem., Int. Ed.* **2016**, *55*, 10686.
[5] X. Zheng, B. Chen, J. Dai, Y. Fang, Y. Bai, Y. Lin, H. Wei, X. C. Zeng, J. Huang, *Nat. Energy* **2017**, *2*, 17102.
[6] a) L. Wang, H. Zhou, J. Hu, B. Huang, M. Sun, B. Dong, G. Zheng, Y. Huang, Y. Chen, L. Li, Z. Xu, N. Li, Z. Liu, Q. Chen, L.-D. Sun, C.-H. Yan, *Science* **2019**, *363*, 265; b) H. Cho, S.-H. Jeong, M.-H. Park, Y.-H. Kim, C. Wolf, C.-L. Lee, J. H. Heo, A. Sadhanala, N. Myoung, S. Yoo, S. H. Im, R. H. Friend, T.-W. Lee, *Science* **2015**, *350*, 1222; c) L. Chen, J. Ou, Z. Liu, H. Lin, H. Wang, J. Dong, H. Zou, *J. Chromatogr. A* **2015**, *1394*, 103; d) L. K. Ono, S. Liu, Y. B. Qi, *Joule* **2018**, *2*, 1961.
[7] a) Z. Hawash, S. R. Raga, D.-Y. Son, L. K. Ono, N.-G. Park, Y. B. Qi, *J. Phys. Chem. Lett.* **2017**, *8*, 3947; b) L. Zuo, Q. Chen, N. De Marco, Y.-T. Hsieh, H. Chen, P. Sun, S.-Y. Chang, H. Zhao, S. Dong, Y. Yang, *Nano Lett.* **2017**, *17*, 269.
[8] Q. Jiang, Y. Zhao, X. Zhang, X. Yang, Y. Chen, Z. Chu, Q. Ye, X. Li, Z. Yin, J. You, *Nat. Photonics* **2019**. *13*, 460.
[9] a) D. Yang, X. Zhou, R. Yang, Z. Yang, W. Yu, X. Wang, C. Li, S. Liu, R. P. H. Chang, *Energy Environ. Sci.* **2016**, *9*, 3071; b) Z. Wu, Z. Liu, Z. Hu, Z. Hawash, L. Qiu, Y. Jiang, L. K. Ono, Y. B. Qi, *Adv. Mater.* **2019**, *31*, 1804284.
[10] C. Stecker, K. Liu, J. Hieulle, R. Ohmann, Z. Liu, L. K. Ono, G. Wang, Y. B. Qi, *ACS Nano* **2019**, *13*, 12127.
[11] Q. Chen, H. Zhou, T.-B. Song, S. Luo, Z. Hong, H.-S. Duan, L. Dou, Y. Liu, Y. Yang, *Nano Lett.* **2014**, *14*, 4158.
[12] J. R. Lakowicz, *Principles of Fluorescence Spectroscopy*, 3rd Ed., Springer, Maryland, USA **2010**.
[13] Q. Dong, Y. Fang, Y. Shao, P. Mulligan, J. Qiu, L. Cao, J. Huang, *Science* **2015**, *347*, 967.
[14] J. Jiménez-López, W. Cambarau, L. Cabau, E. Palomares, *Sci. Rep.* **2017**, *7*, 6101.
[15] X. Zheng, H. Chen, Q. Li, Y. Yang, Z. Wei, Y. Bai, Y. Qiu, D. Zhou, K. S. Wong, S. Yang, *Nano Lett.* **2017**, *17*, 2496.
[16] K. Endo, C. Inoue, N. Kobayashi, M. Aida, *J. Phys. Chem. Solids* **1994**, *55*, 471.
[17] D. G. Castner, K. Hinds, D. W. Grainger, *Langmuir* **1996**, *12*, 5083.
[18] V. d. Vigneaud, C. Ressler, C. J. M. Swan, C. W. Roberts, P. G. Katsoyannis, S. Gordon, *J. Am. Chem. Soc.* **1953**, *75*, 4879.
[19] C. D. Wagner, A. V. Naumkin, A. Kraut-Vass, J. W. Allison, C. J. Powell, J. R. Rumble Jr., NIST Standard Reference Database 20, Version 3.4 (web version) (http://srdata.nist.gov/xps/) (accessed: August 2019).
[20] Y. Huang, L. Li, Z. Liu, H. Jiao, Y. He, X. Wang, R. Zhu, D. Wang, J. Sun, Q. Chen, H. Zhou, *J. Mater. Chem. A* **2017**, *5*, 8537.
[21] D. Yang, R. Yang, K. Wang, C. Wu, X. Zhu, J. Feng, X. Ren, G. Fang, S. Priya, S. Liu, *Nat. Commun.* **2018**, *9*, 3239.